SOFT PHYSICS OF p+Pb AND Pb+Pb COLLISIONS FROM THE ATLAS EXPERIMENT AT THE LHC*

Tomasz Bold

on behalf of the ATLAS Collaboration

AGH University of Science and Technology
al. Mickiewicza 30, 30-059 Kraków, Poland

(Received April 24, 2014)

Physics studies of p+Pb and Pb+Pb collisions in the ATLAS experiment at the LHC range from the studies of a relatively soft sector to the studies of the products of the hard scatterings. In the sector of low transverse momenta, the main areas of interest are the charged particle multiplicities and their scaling with the number of participating nucleons. The collective phenomena arising from the initial collision shape and maintained by the hydrodynamical system evolution from the initial hard scattered quarks and gluons to the hadronized particles are also studied in detail. Recent ATLAS results on the total charged particle multiplicities and spectra in p+Pb are reviewed. The observation of elliptic flow in p+Pb is also presented supplemented with the novel results on the flow coefficients fluctuations and their relation to the initial state of Pb+Pb collisions.

DOI:10.5506/APhysPolB.45.1311
PACS numbers: 12.38.Mh, 25.75.Ld

1. Introduction

In the years 2010–2013, a fraction of the LHC operation time was devoted to heavy-ion programme. In addition to the ALICE detector, other three main LHC experiments took the data with ATLAS [1] among them. Over that time about, $7\,\mu\mathrm{b}^{-1}$ in 2010 and $158\,\mu\mathrm{b}^{-1}$ in 2011 of Pb+Pb collision data at $\sqrt{s_{NN}} = 2.76\,\mathrm{TeV}$ and about $30\,\mathrm{nb}^{-1}$ of p+Pb collisions at $\sqrt{s_{NN}} = 5.02\,\mathrm{TeV}$ in 2013 were recorded by ATLAS. The preliminary results, presented here, are based on $1\,\mu\mathrm{b}^{-1}$ of p+Pb collision data recorded during a pilot run in 2012 and Pb+Pb data from 2010.

* Presented at the Cracow Epiphany Conference on the Physics at the LHC, Kraków, Poland, January 8–10, 2014.

The studies of heavy ion collisions aim to elucidate the properties of hot and dense quark–gluon plasma, QGP, discovered at the RHIC [2–4]. Compared to RHIC the ~ 10 fold increase of the collision energy at the LHC resulted in an increased volume, lifetime and temperature of the QGP [5].

The ATLAS experiment has measured the charged particle production as a function of collision centrality (a proxy to the QGP volume), transverse momenta, p_{T}, and pseudorapidity, η, in p+Pb collisions as they are essential to establish a reference for Pb+Pb collisions [6]. The surprising finding of the studies of p+Pb collisions so far was an observation of the collective phenomena comparable in magnitude to those of Pb+Pb collisions.

2. Centrality of p+Pb collision

In ATLAS, the p+Pb collision centrality has been determined, similarly to the centrality of Pb+Pb collisions, with the use of sum of transverse energy in the forward calorimeter, FCal, covering the pseudorapidity range from 3.2 to 4.8 in the Pb-going direction (direction of Pb beam) denoted as $\Sigma E_{\mathrm{T}}^{\mathrm{Pb}}$. All events are categorised into centrality classes according to their value of $\Sigma E_{\mathrm{T}}^{\mathrm{Pb}}$, as shown in Fig. 1, assuming that the 2% trigger inefficiency is restricted to the lowest $\Sigma E_{\mathrm{T}}^{\mathrm{Pb}}$ [7]. The Glauber and Glauber–Gribov [8] modellings have been used in order to obtain a physical quantity comparable among experiments and theory, namely the number of nucleons participating in the collision, N_{part}. The essential difference of the models is an assumption concerning the fluctuations of the proton–nucleon cross-section in elementary collisions. In the standard Glauber model it is constant, while in the Glauber–Gribov it is allowed to fluctuate. In contrary to Pb+Pb,

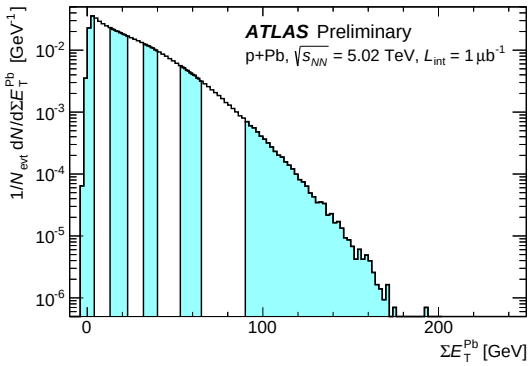


Fig. 1. The distribution of the total transverse energy deposited in the forward calorimeters in the Pb-going direction, $\Sigma E_{\mathrm{T}}^{\mathrm{Pb}}$, for the minimum bias p+Pb data. Shading shows sample splitting into the centrality classes [7].

the cross-section fluctuation plays a significant role in p+Pb, as in a single collision the averaging applies to a lesser extent. In each centrality bin, the distributions of N_{part} are chosen to best approximate the distribution of $\Sigma E_{\mathrm{T}}^{\mathrm{Pb}}$ which results in different mean values (and widths) of N_{part} in each bin of centrality as shown in Fig. 2.

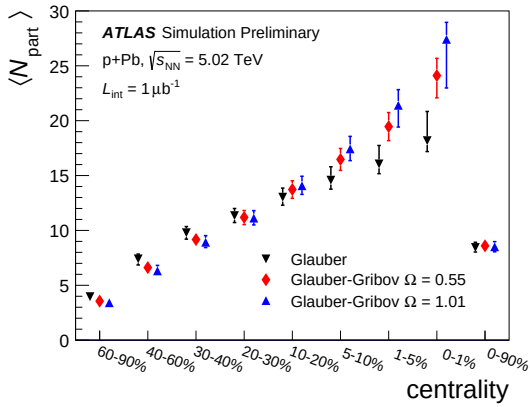


Fig. 2. The number of nucleons participating in the collision for classes of centrality defined by $\Sigma E_{\mathrm{T}}^{\mathrm{Pb}}$ for the two models described in the text. The Ω parameter of the Glauber–Gribov model determines magnitude of the cross-section fluctuations [7].

3. Charged particles centrality, transverse momenta and pseudorapidity dependence in p+Pb collisions

In order to obtain a reliable estimate of the charged particles multiplicity, the tracklets method reaching very low p_{T} has been used. The method, previously applied to Pb+Pb collisions [6], is based on the reconstruction of charged particle tracks with the use of the vertex and only two hits from the ATLAS Pixel detector. For comparison, reconstruction of tracks using all hits from the Pixel detector was also performed. A universal correction including reconstruction inefficiency and detector acceptance effects was obtained from the HIJING MC and GEANT4 detector simulation [7], using the distributions shown in Fig. 3. After applying it, a good agreement of reconstructed $dN_{\mathrm{ch}}/d\eta$ from the two variants of tracklets method and the pixel tracks metod is observed in Fig. 3.

Resulting distributions of $dN_{\mathrm{ch}}/d\eta$, shown in Fig. 4 for the most peripheral collisions are similar to those of p+p collisions [9]. Towards more central collisions, the $dN_{\mathrm{ch}}/d\eta$ becomes more asymmetric, with more particles produced in the Pb-going direction. In the ratio of particle densities in central to peripheral collisions, shown in Fig. 4, the double peak structure vanishes and

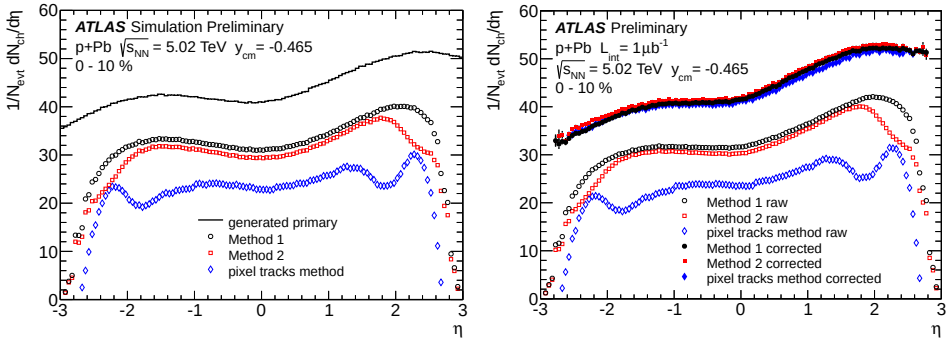


Fig. 3. (left) From the MC simulations: the $dN_{\rm ch}/d\eta$ distribution of generated particles and tracks reconstructed with the three tracking methods without inefficiency or acceptance corrections. (right) From the data: the $dN_{\rm ch}/d\eta$ distributions from the three tracking methods before and after applying the inefficiency and acceptance corrections. In both cases the most central 0–10% events were used [7].

the ratios are almost linear functions of η with the slope parameter growing with centrality. The $dN_{\rm ch}/d\eta$ divided by the number of participant nucleons has been measured in bins of pseudorapidity as shown in Fig. 5. The $\langle N_{\rm part}\rangle$ estimate has been obtained with the use of the three aforementioned implementations of the Glauber model. Flat dependence up to 10 participants is observed. In the Pb-going side the charged particle multiplicity evolves

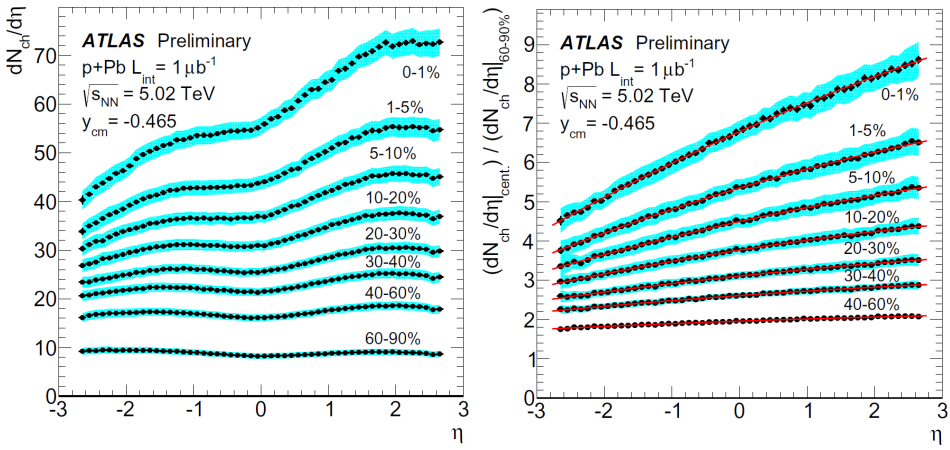


Fig. 4. (left) The distribution of the charged particles multiplicity, $N_{\rm ch}$, per unit of pseudorapidity, η, as a function of pseudorapidity in bins of centrality as labeled. (right) The ratio of the $dN_{\rm ch}/d\eta$ distributions in a bin of centrality to the most peripheral bin 60–90% as described by the labels [7].

differently with the $\langle N_{\text{part}} \rangle$ than in the p-going direction. The dependence of scaled multiplicity on N_{part} is different for the models considered, thus the interpretation depends on modelling of the proton–nucleus collisions.

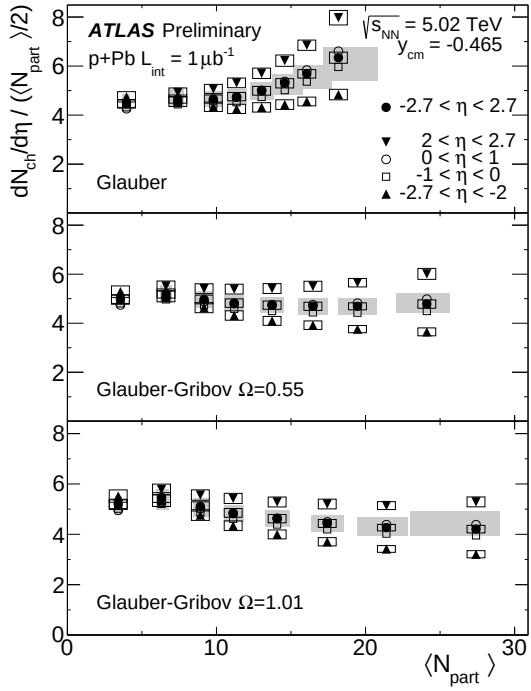


Fig. 5. The mean values of $dN_{\text{ch}}/d\eta$ in several ranges of pseudorapidity as a function of the mean number of participants, $\langle N_{\text{part}} \rangle$, estimated with the three Glauber model implementations [7].

The transverse momentum, p_{T}, spectra of charged particles in p+Pb collisions have also been studied by ATLAS [10]. For this purpose, the default track reconstruction method with good p_{T} resolution has been used. The lowest p_{T} reached is 0.1 GeV. Figure 6 shows examples of the charged particle spectra in either bins of centrality or in bins of rapidity. The rapidity of the charged particles, y^*, in the proton–nucleus rest frame was calculated from the particle emission angle assuming that the particle has the pion mass, and shifted by the rapidity of the proton–nucleus centre of mass $y_{\text{CM}} = -0.465$. The p+Pb spectra were compared with the $p + p$ results, which were scaled by the nuclear thickness factor $\langle T_{\text{Pb}} \rangle$ obtained with the Glauber model. The p+p cross-section, σ_{pp}, was interpolated from the measurements at the 2.76 TeV and 7 TeV. In order to better illustrate the change of the

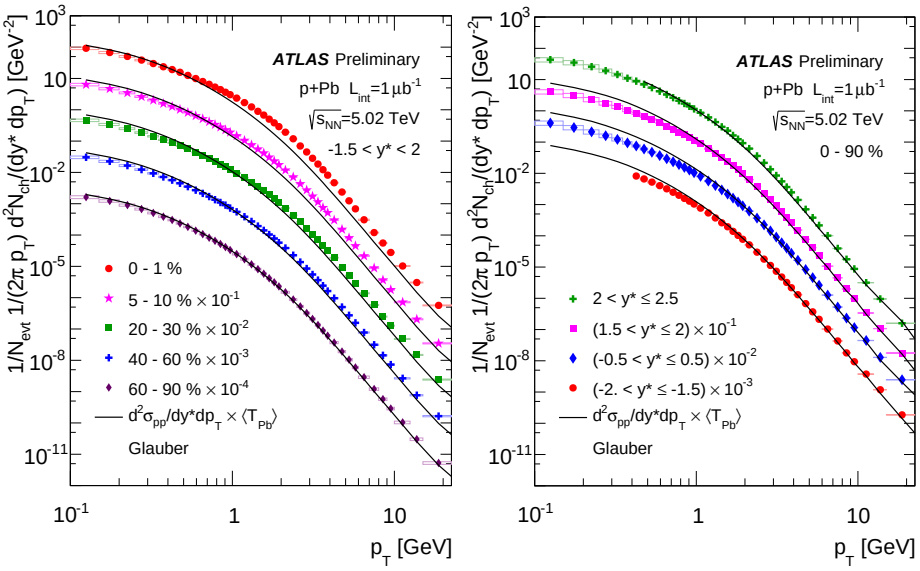


Fig. 6. (left) The invariant distribution of charged particles transverse momentum, p_{T}, in rapidity range from -1.5 to 2 in five bins of centrality. (right) The invariant distribution of charged particles transverse momentum averaged over the range of collision centrality 0–90% in four bins of rapidity. The distributions were scaled down by powers of ten as denoted in the legend in order to assure readability. Lines superimposed on data points are extrapolations of appropriately scaled $p+p$ spectra [10].

spectra, the nuclear modification factor

$$R_{p\mathrm{Pb}} = \frac{1}{\langle T_{\mathrm{Pb}} \rangle N_{\mathrm{evt}}} \frac{d^2 N_{p+\mathrm{Pb}}/dy^* dp_{\mathrm{T}}}{d^2 \sigma_{pp}/dy^* dp_{\mathrm{T}}},$$

is used. Several examples of R_{Pb} dependence on p_{T} for different centralities, rapidity ranges, and Glauber model implementations used to calculate $\langle T_{\mathrm{Pb}} \rangle$ are shown in Fig. 7. Irrespectively of the model used, the suppression of $R_{p\mathrm{Pb}}$ at the very low p_{T} is observed. It is stronger in the p-going direction and is visible even for most peripheral collisions. The peak structure at the $p_{\mathrm{T}} \simeq 2\,\mathrm{GeV}$ is attributed to the Cronin effect. The suppression at higher p_{T} appears only for the Glauber–Gribov models which predict larger values of $\langle T_{\mathrm{Pb}} \rangle$. In Fig. 8 the $R_{p\mathrm{Pb}}$ values obtained in a wide, 0–90%, range of centrality for $\eta \approx 0$ from the ATLAS and ALICE [11] experiments are compared.

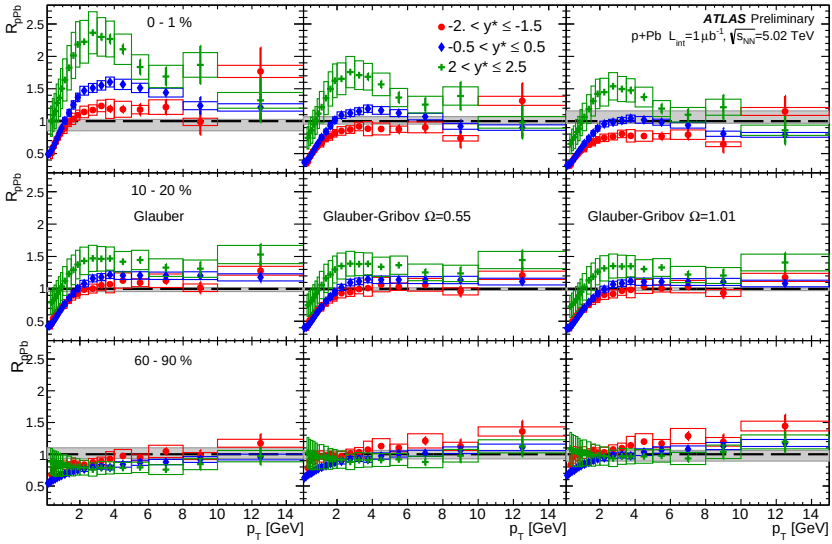


Fig. 7. The nuclear modification factor, $R_{p\mathrm{Pb}}$, in three ranges of rapidity y^* for the Glauber model (left column) and Glauber–Gribov with different values of cross-section fluctuation parameter Ω (center and right columns) in the bins of centrality from 1% most central collisions (top), central 10–20% (middle) and peripheral 60–90% (bottom) [10].

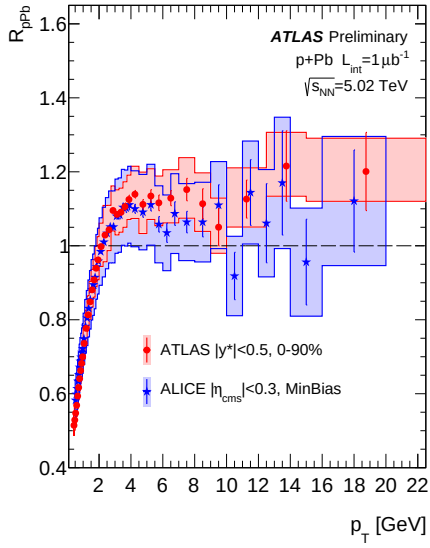


Fig. 8. $R_{p\mathrm{Pb}}$ in the rapidity range $|y^*| < 0.5$ averaged over centrality range 0–90% as a function of p_{T} from the ATLAS and ALICE [11] experiments. The Glauber model has been used from modelling of the $\langle T_{\mathrm{Pb}} \rangle$ [10].

4. Collective behaviour in Pb+Pb and p+Pb collisions

It is known that relativistic hydrodynamic models describe well the evolution of the QGP. These models predict existence of anisotropies in the particles emission as a result of very low viscosity of the medium. The asymmetry of the initial collision region is transfered largely intact to the stage of the hadronization and can be observed as anisotropy of azimuthal distributions of particles.

The quantitative parameters used to describe the anisotropy are the Fourier expansion coefficients, v_n

$$dN_{\mathrm{ch}}/d\phi \propto 1 + \sum_n v_n \cos\left[n\left(\phi - \Psi_n\right)\right] ,$$

where ϕ is the azimuthal angle of a particle with respect to the n^{th} symmetry plane, orientation of which is given by Ψ_n. Since the shape of the collision area vary from event to event, even with the same N_{part}, the experimental observable, v_n, fluctuates accordingly. Only recently, it has been realised that the fluctuations of v_n are sizeable and they affect the measured quantities in a non-trivial way [12].

Large multiplicity of charged particles available in Pb+Pb collisions at the LHC, allows to measure the v_2, v_3 and v_4 coefficients on the event-by-event basis and assess directly the magnitude of the fluctuations [13]. Examples of per event azimuthal anisotropy are shown in Fig. 9. The analysis is based on a measurement of the $\vec{v}_n = \langle\cos(n\phi)\rangle, \langle\sin(n\phi)\rangle$ vector in every event using charged particle tracks. The probability distribution of the density of $\vec{v}_n$, relative to the reaction plane, can be approximated by a two-dimensional Gaussian function. It is azimuthally symmetric, thus, in the study of flow fluctuations the magnitude of $\vec{v}_n$ vector, $v_n = |\vec{v}_n|$ is used. After an integration of the 2D Gaussian distribution over the azimuthal dimension, the v_n distribution becomes the Bessel–Gauss distribution

$$p(v_n) = \frac{v_n}{\delta^2_{v_n}} I_0\left(\frac{v_n^{\mathrm{RP}} v_n}{\delta^2_{v_n}}\right) \exp\left(\frac{\left(v_n^{\mathrm{RP}}\right)^2 - v_n^2}{2\delta^2_{v_n}}\right) ,$$

where the δ_{v_n} is a width of the distribution, v_n^{RP} is mean orientation of the symmetry plane and I_0 is modified Bessel function of the first kind. The 2D distribution of $\vec{v}_2$ and the result of integration are shown in Fig. 10. The raw v_n distributions are smeared due to limited statistics in Gaussian manner. The response function connecting v_n and v_n^{obs} has been obtained from the distributions of the difference between v_n values calculated in the same events using tracks with $\eta < 0$ and $\eta > 0$. The iterative deconvolution technique has been applied in order to recover the true distributions of v_n.

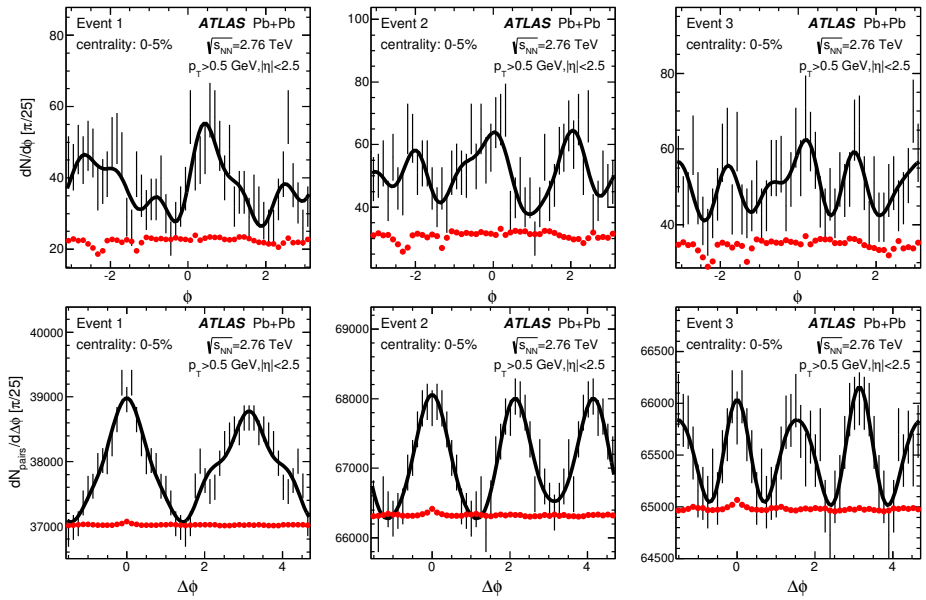


Fig. 9. (top row) The charged particle density in azimuthal angle, ϕ, in the laboratory frame, $dN_{\rm ch}/d\phi$ (black points) for three typical central collisions. (bottom row) The $dN_{\rm pairs}/d\Delta\phi$ as a function of the difference between azimuthal angles for pairs of tracks, $\Delta\phi$, for the same three central events. The grey/red points represent the same quantities averaged over many events. The fitted Fourier series are shown as black lines [13].

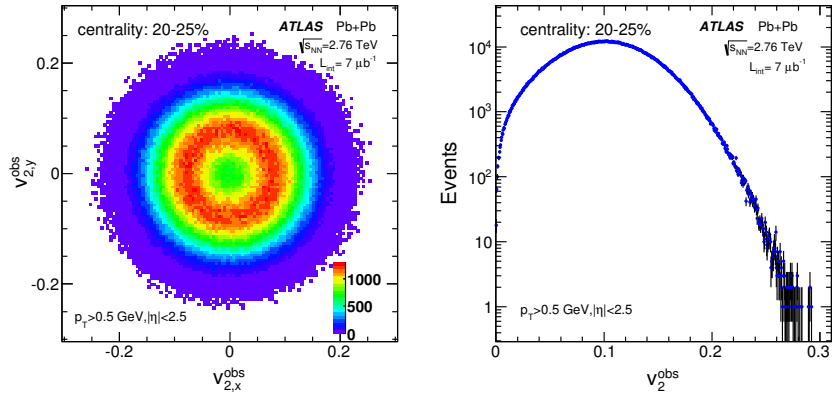


Fig. 10. The distribution of $\vec{v}_2$ (left) and v_2 in the centrality bin 20–25% [13].

It can be noticed that the fits to the data points support the hypothesis of the Gaussian fluctuations of the shape as the source of the azimuthal anisotropies. This is the case for the most central collisions for v_2 and almost for the entire range of centralities for v_3 and v_4, as shown in Fig. 11.

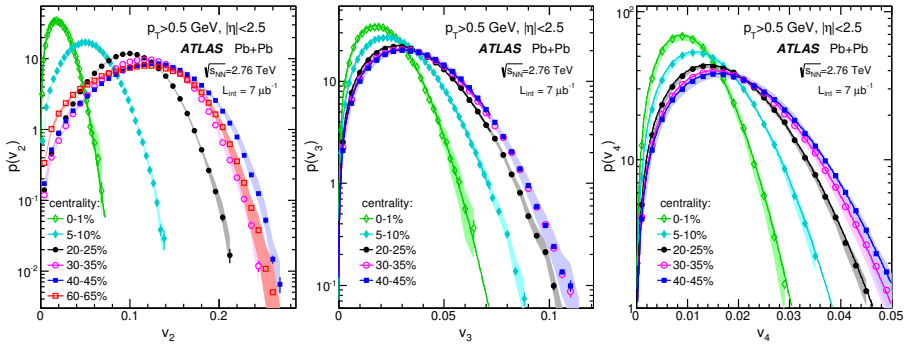


Fig. 11. The distribution of v_2, v_3 and v_4 in Pb+Pb collisions in six bins of centrality. Superimposed on top, with the same colour, are the Bessel–Gauss function fitted to the data [13].

When the fluctuations, characterised by the width δ_{v_n}, are small, $\delta_{v_n} \ll v_n^{\mathrm{RP}}$, the v_n^{RP} can be approximated as

$$\left(v_n^{\mathrm{RP}}\right)^2 = \langle v_n \rangle^2 - \delta_{v_n}^2 \,.$$

On the other hand, when the fluctuations width δ_{v_n} is significantly higher than the v_n^{RP}, for instance in the central collisions, the $p(v_n)$ reduces to

$$p(v_n) = \frac{v_n}{\delta_{v_n}^2} \exp\left(\frac{-v_n^2}{2\delta_{v_n}^2}\right) .$$

The ratio of dispersion, σ_{v_n}, to the mean value of this distribution reaches in this case the maximal value

$$\frac{\sigma_{v_n}}{\langle v_n \rangle} = \sqrt{4/\pi - 1} \simeq 0.523 \,.$$

Study of this fraction can be used to quantify the relative magnitude of fluctuations and is shown in Fig. 12. The $\langle v_n \rangle$ and σ_{v_n} decrease as we move from peripheral to central collisions. Both observables depend on the p_{T} range of studied particles, while the ratios $\sigma_{v_n}/\langle v_n \rangle$ are almost independent of the choice of p_{T}. The ratios suggest that the v_n in the central collisions arise from the fluctuations only. In more peripheral collisions, the hypothesis of the collision shape fluctuations as the source of the v_n is confirmed for $n > 2$ up to the most peripheral collisions studied. Only values of the second harmonics, v_2, are dominated by the mean collision geometry represented by v_2^{RP} ($v \to 2$). The results of the MC simulations fail to describe the v_2, while work better for v_3 and v_4.

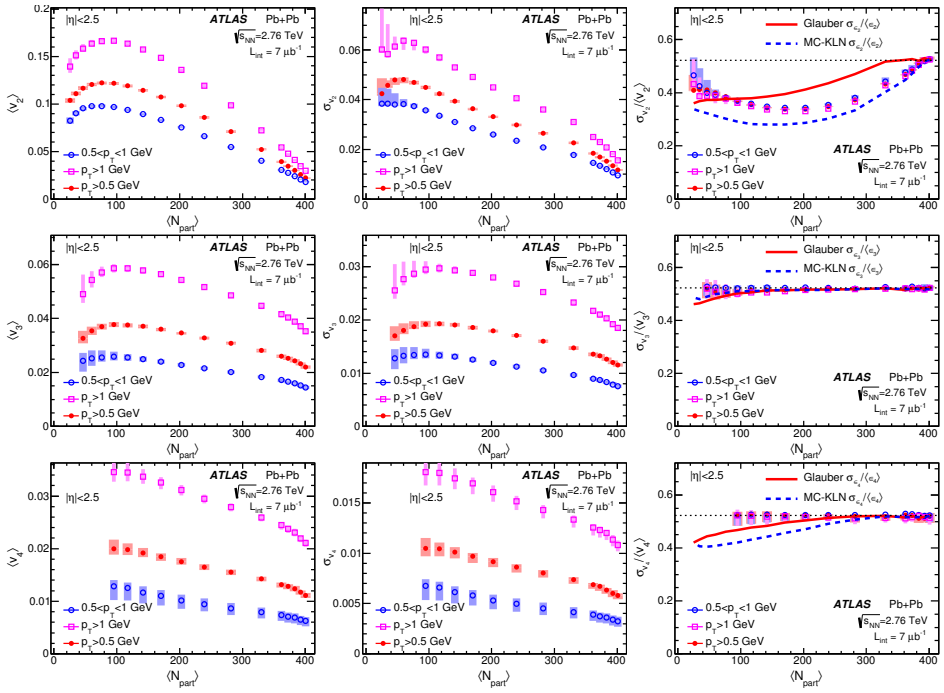


Fig. 12. (left) The mean value of the v_2 (top), v_3 (middle) and v_4 (bottom) distributions for charged particles in three ranges of p_{T}, as a function of number of participants. (center) The dispersion, σ_{v_n}, of the v_n distributions in ranges of p_{T} as in the left column. (right) Ratio $\sigma_{v_n}/\langle v_n \rangle$, in data (points) compared to the same quantity obtained from MC simulations (lines) as a function of the number of participants [13].

The v_2 coefficient has also been measured in p+Pb collisions [14, 15]. The presence of the collective behaviour and, in consequence, significant anisotropy has been suggested by the hydrodynamical modelling [16] even if the dimensions of the produced system, compared to the mean free paths of the interacting partons, are much smaller than in Pb+Pb collisions. Assuming that anisotropy arises from the fluctuations of the shape of the volume occupied by the participating nucleons in the Pb nuclei, the magnitude of the anisotropy should be independent of the collision centrality. This is confirmed by the measurements shown in Fig. 13. Also the comparison of the anisotropy in p+Pb and Pb+Pb collisions, shown in Fig. 14, suggests that v_2 observed in the former is due to the fluctuations of the shape, however some average collision geometry influence cannot be excluded.

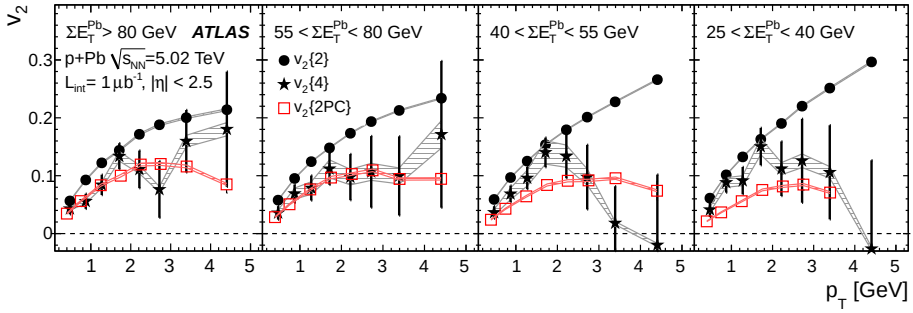


Fig. 13. The p_{T} dependence of v_2 in bins of centrality defined by ranges of $\Sigma E_{\mathrm{T}}^{\mathrm{Pb}}$. Three methods of estimating v_2 are shown with different symbols, $v_2\{2\}$ from two particle cumulants, $v_2\{4\}$ from four particle cumulants and $v_2\{2\mathrm{PC}\}$ from two particle correlations [14].

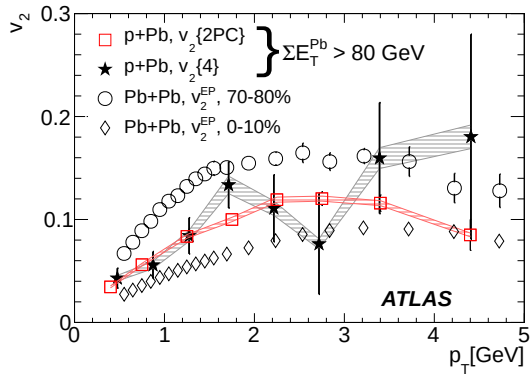


Fig. 14. The comparison of the p_{T} dependence of v_2 in central p+Pb collisions obtained from the two particle correlations, $v_2\{2\mathrm{PC}\}$, and from the four-particle cumulants, $v_2\{4\}$, with that in central and peripheral Pb+Pb collisions obtained using the event plane method, v_2^{EP} [14].

5. Summary

The ATLAS experiment, profiting from high-quality tracking detectors covering five units in pseudorapidity, performs measurements involving particles with low transverse momenta. Recently, preliminary measurements of charged particle multiplicities in p+Pb collisions as a function of collision centrality and pseudorapidity have been performed. The significant asymmetry of $dN_{\mathrm{ch}}/d\eta$, growing with the centrality, has been found. The measured spectra confirm an expected structure of the nuclear suppression factor

at low p_{T} however uncertainty related to possible fluctuations of proton–nucleon cross-section does not allow to quantify the suppression at higher transverse momenta of charged particles. Detailed, event-by-event, measurements of the flow phenomena in Pb+Pb collisions point to the origin of the higher harmonic modes, $v_{n>2}$, in the azimuthal charged particles emission anisotropy identified as shape fluctuations of the collision overlap region. The preliminary measurements of v_2 in the p+Pb collisions suggest that it has the same origin, namely the shape fluctuations of the initial positions of wounded nucleons in the Pb system.

This work was supported in part by the Polish National Science Center grants DEC-2011/03/B/ST/02631, DEC-2013/08/M/ST2/00320 and by PL-Grid Infrastructure.

REFERENCES

[1] ATLAS Collaboration, *JINST* **3**, S08003 (2008).
[2] J. Adams *et al.*, *Nucl. Phys.* **A757**, 102 (2005).
[3] B. Back *et al.*, *Nucl. Phys.* **A757**, 28 (2005).
[4] I. Arsene *et al.*, *Nucl. Phys.* **A757**, 1 (2005).
[5] C.A. Salgado, *Nucl. Phys.* **A774**, 267 (2006).
[6] ATLAS Collaboration, *Phys. Lett.* **B710**, 363 (2012).
[7] ATLAS Collaboration, `https://cds.cern.ch/record/1599773`
[8] V. Guzey, M. Strikman, *Phys. Lett.* **B633**, 245 (2006).
[9] ATLAS Collaboration, *New J. Phys.* **13**, 053033 (2011).
[10] ATLAS Collaboration, `https://cds.cern.ch/record/1624333`
[11] ALICE Collaboration, *Phys. Rev. Lett.* **110**, 082302 (2013).
[12] B. Alver, G. Roland, *Phys. Rev.* **C81**, 054905 (2010).
[13] ATLAS Collaboration, *J. High Energy Phys.* **1311**, 183 (2013).
[14] ATLAS Collaboration, *Phys. Lett.* **B725**, 60 (2013), and auxiliary material from `https://atlas.web.cern.ch/Atlas/GROUPS/PHYSICS/PAPERS/HION-2013-01/`
[15] ATLAS Collaboration, *Phys. Rev. Lett.* **110**, 182302 (2013).
[16] P. Bozek, W. Broniowski, *Phys. Lett.* **B718**, 1557 (2013).